Atomistic Mechanism of Force Generation, Translocation, and Coordination in a Viral Genome Packaging Motor

Joshua Pajak[1,‡], Erik Dill[2,‡], Mark A. White[3], Brian A. Kelch[4], Paul Jardine[5,†], Gaurav Arya[1,†], and Marc C. Morais[2,3,†]

1. Dept. of Mechanical Engineering and Materials Science, Duke University, Durham, NC 27708
2. Dept. of Biochemistry and Molecular Biology, University of Texas Medical Branch, Galveston, TX 77550
3. Sealy Center for Structural Biology and Molecular Biophysics, University of Texas Medical Branch, Galveston, TX 77555, USA
4. Dept. of Biochemistry and Molecular Pharmacology, University of Massachusetts Medical School, Worcester, MA 01605
5. Dept. of Diagnostic and Biological Sciences, University of Minnesota, Minneapolis, MN 55455

Summary

Double-stranded DNA viruses package their genomes into pre-assembled protein capsids using virally-encoded ATPase ring motors. While several structures of isolated monomers (subunits) from these motors have been determined, they provide little insight into how subunits within a functional ring coordinate their activities to efficiently generate force and translocate DNA. Here we describe the first atomic-resolution structure of a functional ring form of a viral DNA packaging motor and characterize its atomic-level dynamics via long timescale molecular dynamics simulations. Crystal structures of the pentameric ATPase ring from bacteriophage asccφ28 show that each subunit consists of a canonical N-terminal ASCE ATPase domain connected to a 'vestigial' nuclease domain by a small lid subdomain. The lid subdomain closes over the ATPase active site and engages in extensive interactions with a neighboring subunit such that several important catalytic residues are positioned to function *in trans*. The pore of the ring is lined with several positively charged residues that can interact with DNA. Simulations of the ATPase ring in various nucleotide-bound states provide information about how the motor coordinates sequential nucleotide binding, hydrolysis, and exchange around the ring. Simulations also predict that the ring adopts a helical structure to track DNA, consistent with recent cryo-EM reconstruction of the φ29 packaging ATPase. Based on these results, an atomistic model of viral DNA packaging is proposed wherein DNA translocation is powered by stepwise helical-to-planar ring transitions that are tightly coordinated by ATP binding, hydrolysis, and release.

[†]Correspondence: jardine@umn.edu, gaurav.arya@duke.edu, mcmorais@utmb.edu

[‡]Co-first authorship

Keywords: ASCE, ATPase, bacteriophage, crystal structure, DNA, DNA packaging, molecular dynamics simulations, molecular motor

Introduction

The Additional Strand, Conserved Glutamate (ASCE) superfamily is an ancient and ubiquitous class of NTPases, encompassing subfamilies such as AAA+ motors, RecA-/FtsK-like ATPases, and ABC transporters (Erzberger and Berger, 2006). These motors convert energy from NTP binding and/or hydrolysis into mechanical work, and typically perform biological segregation tasks such as proton transport, chromosomal segregation, DNA or RNA strand separation, and protein degradation. The multimeric ring motors that drive genome packaging in viruses highlight the power and processivity that can arise from the coordinated activity of individual subunits in ASCE ATPases. Double-stranded DNA (dsDNA) viruses, such as herpes-, adeno-, and pox viruses, as well all tailed bacteriophages, code for ASCE segregation motors that they use to package their genomes into preformed procapsids during virus replication (Casjens, 2011; Morais, 2012; Rao and Feiss, 2015). Among ASCE ATPases, viral packaging motors generate particularly high forces to overcome the entropy loss, electrostatic repulsion, and DNA stiffness that oppose DNA confinement (Fuller et al., 2007a, 2007b; Pajak et al., 2019; Smith et al., 2001). Thus, viral dsDNA packaging motors provide a unique window into the mechanochemistry of force-generation found in this broad class of molecular motors.

Single-molecule force spectroscopy (SMFS) experiments have provided valuable information on force-generation and dynamics of viral packaging motors. SMSF studies on bacteriophages T4 (Fuller et al., 2007b), λ (Fuller et al., 2007a), and φ29 (Smith et al., 2001) demonstrated that viral DNA packaging motors can generate more than 50 pN of force, roughly an order of magnitude larger than the amount of force generated by the familiar myosin and kinesin motors (Finer et al., 1994; Svoboda et al., 1993). Although each of these phages generate similar maximum forces, the measured average rate of DNA translocation can vary by an order of magnitude, from 2,000 base pairs/second (bp/s) for T4 to 200 bp/s for φ29. At least partially due to its slower translocation rate, φ29's mechano-chemical cycle has been amenable to detailed dissection via SMSF studies. To briefly summarize, high-resolution optical laser tweezer measurements showed that the φ29 packaging motor translocates DNA in a highly coordinated punctuated fashion. Specifically, the motor packages DNA in 10 bp "bursts" comprised of four 2.5 bp sub-steps, each coupled to ATP hydrolysis and phosphate release. DNA translocation bursts are followed by a relatively long "dwell" wherein DNA translocation pauses while each ADP is sequentially exchanged for ATP to reset the motor for the next burst (Chistol et al., 2012; Moffitt et al., 2009). Finally, experiments with altered DNA substrates showed that the motor primarily tracks DNA along one of the strands, and makes critical electrostatic contacts with pairs of phosphates every 10 bp (Aathavan et al., 2009).

In addition to being well suited for SMSF studies, the relatively small size and simplicity of φ29 has facilitated advanced genetic, biochemical, and structural studies (Morais, 2012). All components of the φ29 packaging system have been thoroughly characterized, and a robust highly efficient in vitro DNA packaging system has been developed (Grimes et al., 2002).Furthermore, atomic resolution structures of all individual φ29 motor components are available (Ding et al., 2011; Mahler et al., 2020; Mao et al., 2016a; Simpson et al., 2000) and medium resolution structures of motors assembled on capsids in various stages of assembly and/or packaging have been determined (Koti et al., 2008; Mao et al., 2016b; Morais et al., 2005, 2008; Simpson et al., 2000; Woodson et al., 2020). These results indicate that the DNA packaging motor consists of a dodecameric portal protein, a pentameric prohead RNA (pRNA), and a pentameric ATPase (gene product 16; gp16) that assemble as co-axial rings at a unique vertex of the φ29 capsid.

Whereas genetic, biochemical, structural, and single-molecule studies have provided significant insights into the mechanochemistry of the φ29 packaging motor, the molecular basis of force-generation and coordination remains unresolved for any viral DNA packaging motor. Given the multi-component nature of the motor, it is difficult to determine how such coordination arises in the

absence of high-resolution quaternary structural information. Likewise, it is difficult to determine the mechanisms of force generation in the absence of atomistic structural dynamics information. Hence, we employed a combined strategy of high-resolution structure determination and long-timescale molecular dynamics (MD) simulations to address these fundamental questions. With this combined approach, we show that: 1) the packaging motors from φ29-like phages can transition between planar-ring and short-helix conformations, 2) these transitions occur in a highly coordinated, nucleotide-dependent fashion, and 3) these transitions provide a plausible, generalizable mechanism for coupling ATP hydrolysis to force-generation in ASCE ATPases.

Results

Rationale for structural target

Despite extensive efforts, it has not been possible to assemble the functional ring-form of the packaging ATPase from bacteriophage φ29 detached from procapsids. This is not surprising, since previous cryo-EM studies have shown that in φ29, gp16 assembles a ring only by virtue of interacting with a pRNA scaffold that binds to the motor vertex of the phage (Morais et al., 2008). Hence, we targeted a homolog of the φ29 ATPase from the φ29 related bacteriophage asccφ28, gp11; since asccφ28 seemingly does not code for pRNA (Kotsonis et al., 2008), we suspected that its ATPase may assemble as rings in solution. Indeed, extensive analytical ultracentrifugation and small-angle X-ray scattering experiments strongly indicated that the ATPase forms pentameric rings (unpublished data). Thus, we used asccφ28 gp11 for crystallographic structure determination since: it forms functional rings in solution amenable to structural and computational analysis; and it is sufficiently similar to φ29 that any structural and computational results on gp11 can be interpreted in light of accumulated data for the φ29 system.

X-ray crystal structure determination

Cloning, protein purification, kinetic analysis, AUC, SAXS, negative stain TEM, and preliminary crystallization of gp11 is not shown, to be deposited on bioRxiv shortly. Briefly, two crystal forms of gp11 were obtained: 1) tetragonal crystals belonging to space group $P4_12_12$ and 2) trigonal crystals belonging to space group $P3_12_1$. Single-wavelength anomalous dispersion (SAD) was used to obtain initial experimental phases for the tetragonal $P3_12_1$ crystals grown from seleno-methionine labeled protein (**Table S1**). The final refined structure was used as a molecular replacement search model to phase the data from the trigonal $P3_12_1$ space group.

Quaternary structure of gp11

The tetragonal and trigonal crystal forms had similar pentameric rings in their crystallographic asymmetric units despite having substantially different packing environments (**Fig. 1**), suggesting that the observed pentamer is the biological assembly. This stoichiometry is consistent with previously reported biochemical and biophysical analysis indicating gp11 forms pentameric rings in solution (data not shown; to be deposited on bioRxiv shortly; data available upon request to MCM). Of note, the kinetic parameters of ATP binding and hydrolysis by isolated gp11 rings are similar to the parameters obtained for φ29 and other bacteriophage DNA packaging motors but only once these other ATPases are assembled as functional rings on their respective procapsids (data not shown; to be deposited on bioRxiv shortly; data available upon request to MCM). In the absence of procapsids, other packaging motors negligibly hydrolyze ATP, presumably since they are in monomeric form and therefore cannot efficiently bind or hydrolyze ATP (see also below). Further, the closely related φ29 packaging ATPase has been definitively shown to assemble as pentamers in functional motors (Koti et al., 2008; Mao et al., 2016b; Morais et al., 2005, 2008; Simpson et al., 2000; Woodson et al., 2020). Hence, the pentameric assembly of gp11 observed here likely reflects a functional assembly during DNA packaging.

Tertiary structure of gp11

Individual subunits within the ring are organized into two globular domains connected by a linker domain. The N-terminal domain adopts the

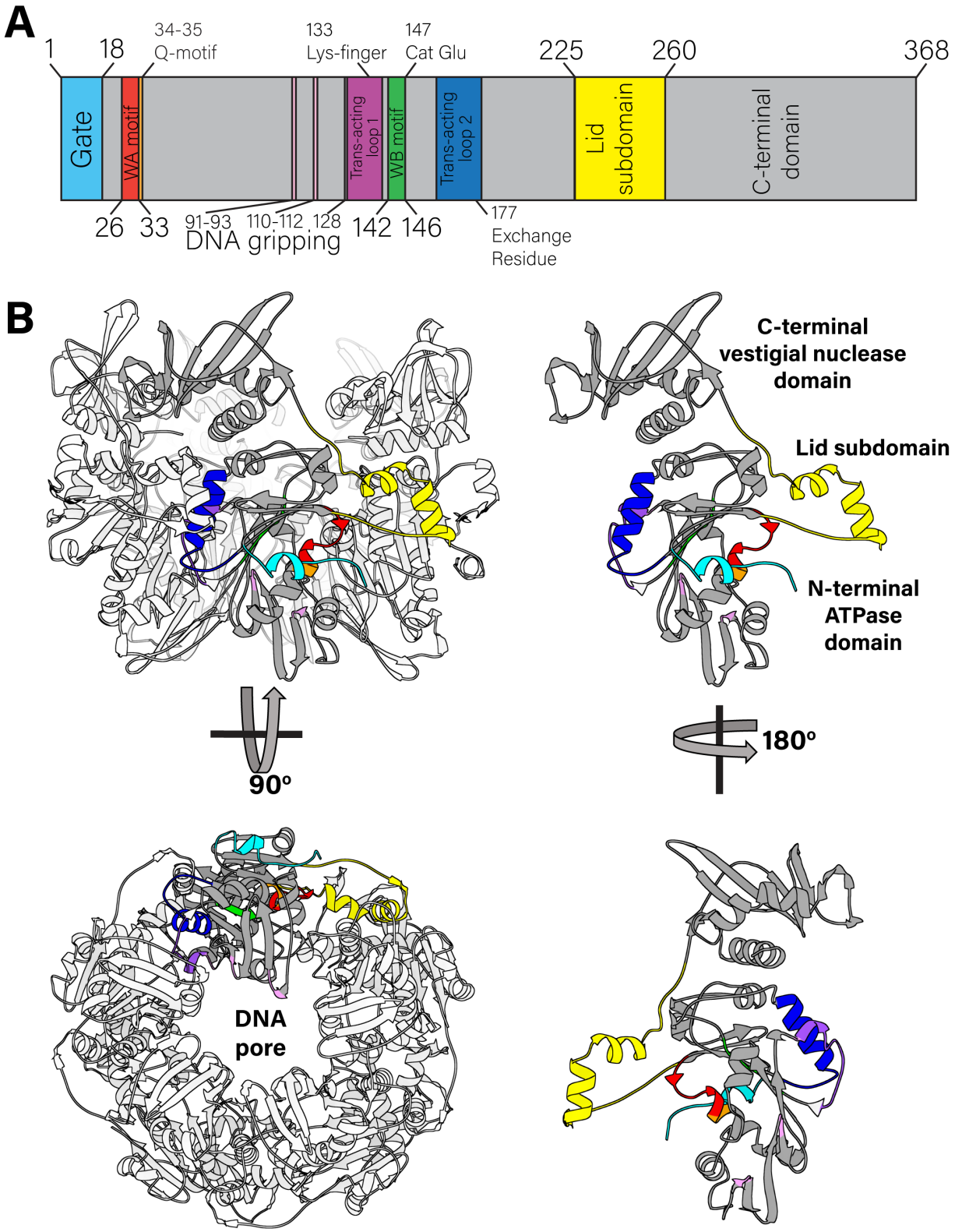

Figure 1: Quaternary and tertiary structure of the asccφ28 packaging ATPase. A. Sequence of the packaging ATPase contains canonical ASCE motifs, such as the Walker A and Walker B motifs. **B.** Structure of the pentamer (left), with a single subunit highlighted in gray and its lid subdomain highlighted in yellow is shown from side and end-on views (top and bottom panels, respectively). The lid subdomain mediates most inter-subunit contacts. The monomer in isolation (right) is color coded to match the motif classification in panel A, and is shown in two side views, from the exterior of the motor (top) and the interior of the lumen (bottom).

canonical ASCE ATPase fold, while the C-terminal domain is a "vestigial nuclease domain" similar to φ29 C-terminal domain (Mahler et al., 2020). The linker domain (residues 225 to 260) adopts a helix-loop-helix fold, reminiscent of the lid subdomain identified in other ASCE ATPases such as AAA+ and helicases (Erzberger and Berger, 2006). This domain arrangement and helix-loop-helix lid subdomain is similar to other viral DNA packaging ATPases, despite exceedingly low sequence homology. However, unlike the monomeric structures of other ATPases, the lid subdomain of the asccφ28 packaging ATPase extends away from the ATPase domain (**Fig. S1**). This difference reflects a change in conformation that the lid domain undergoes upon oligomerization into a functional ring. In monomeric structures the polypeptide region that connects the ATPase and lid subdomain folds into a more compact structure, likely due to a lack of opportunity to interact with a neighboring subunit in the same manner. In contrast, in the oligomeric ring structures observed here, this polypeptide region is almost completely extended, allowing the lid domain to make extensive interactions with the neighboring subunit. Thus, we predict that the lid subdomains observed in monomers of packaging ATPases would undergo a conformational change to similarly extend and interact with neighboring subunits upon oligomerization into functional ATPase rings.

Interactions promoting ring assembly

In the ring structures of gp11 presented here, the lid subdomain is predominantly positively charged, whereas the region it interacts with on the neighboring subunit is mostly negatively charged (**Fig. S2**). This creates a "Velcro-like" pattern of complementary sticky patches that promotes oligomerization into a ring-like structures, and thus likely helps to direct coordination between adjacent subunits. Although oligomeric structures are not available for other packaging ATPases, this complementary pattern of surface-charge distribution is present in the solved structures of monomers, suggesting that these packaging ATPases would form functional rings via similar inter-subunit interactions. For example, in the bacteriophage D6E packaging ATPase, the same pattern and polarity of surface-charge complementarity is observed (**Fig. S2**). In the bacteriophage T4 packaging ATPase, the pattern is conserved, but polarity is reversed; the lid subdomain is negatively charged, and the corresponding binding patch is positively charged (**Fig. S2**). Further, similar complementary charge patches between the lid subdomain and the neighboring subunit are present in ring ATPases residing on other branches of the ASCE evolutionary tree, such as katanin (Zehr et al., 2017), ClpX (Glynn et al., 2009), and Vsp4 (Han et al., 2019). Despite assembling as hexamers rather than pentamers, analogous interactions promote assembly (**Fig. S2**). Thus, this pattern of sticky patches may be a generic feature common among many ringed NTPases to promote functional ring formation and inter-subunit coordination.

ATPase active site: *cis*- contributions

While the three structures described here were determined in the absence of nucleotide, the active sites of ASCE ATPases are well characterized, and can be accurately identified via comparisons with other ATPase structures determined in the presence of nucleotide. Comparison with the packaging ATPase from phage P74-26 (Hilbert et al., 2015) positions the asccφ28 gp11 ATPase active site between two subunits, such that a single active site consists of multiple components from two adjacent subunits. The *cis*-acting side of the ATP-binding interface resides on one edge of the central beta-sheet of the Rossmann fold and includes canonical Walker A (26-GGRGVGKT-33) and Walker B (142-YLVFD-146) motifs. The active-site region superimposes well onto the solved structures of the φ29, T4, Sf6, P74-26, and D6E bacteriophage packaging ATPase domains.

Two distinct conformations of the Walker A motif (**Fig. S3**) are apparent in our crystal structures. One conformation binds either a SO_4^{2-} or PO_4^{3-} ion in the canonical β-phosphate position. The ion forms hydrogen bonds with the backbone of the Walker A motif in lieu of a β-phosphate, typically provided by ATP or ADP, which explains why the Walker A backbone adopts a conformation similar

to a typical nucleotide-bound ATPase configuration. However, because the structure was solved in absence of nucleotide or nucleotide analog, it lacks any interactions mediated by the α- and γ-phosphates, ribose sugar, or adenosine base. Thus, this structure likely represents a conformation with mixed characteristics from both the apo and nucleotide-bound configurations.

In contrast, the conformation observed in the iodine-bound structure shows that an iodine atom sits in a hydrophobic pocket that is occupied by Val30 in the structures determined in the absence of iodine. As a result of displacing this Val30, the Walker A motif must adopt an extra helical turn in the phosphate-binding loop. This conformational change excludes the possibility of binding nucleotide since: 1) the sidechain of Val30 is in the center of the active site, occluding nucleotide, and 2) the Walker A NH-groups are repositioned such that they can no longer hydrogen bond with the β-phosphate. Initially, we assumed that the nucleotide-blocking valine in the iodine structure was an artifact of heavy atom derivatization. However, subsequent structural analysis and MD simulations indicated that the two conformations of this loop may reflect an ability to switch between nucleotide accepting and occluding conformations, providing a mechanism for regulation of ATP binding and ADP release (see also below).

ATPase active site: *trans*- contributions

The *trans*-acting side of the subunit interface consists primarily of two helical segments (residues 129-139 and 161-178) that reside on the side of the central beta sheet opposite the *cis*-contributing elements. These helices position polar- and positively-charged residues in the 'neighboring' active site that likely contribute to ATP binding and hydrolysis, as well as to phosphate and ADP release (**Fig. 1**). Notably, Arg177 is positioned in the active site of all three crystal structures. Arg177 in asccφ28 corresponds to Arg146 in the phage φ29 ATPase, which had previously been identified as a *trans*-acting arginine finger based on bioinformatics, structural, kinetic, and single-molecule data (Mao et al., 2016a; Tafoya et al., 2018). Arginine finger motifs are ubiquitous in ring ATPases and are generally believed to catalyze ATP hydrolysis by providing a positive charge that stabilizes the negative charge that accumulates on the γ-phosphate oxygens during the hydrolytic transition state (Ogura et al., 2004). However, the sidechain of Arg177 is not optimally positioned to coordinate the expected position of the γ-phosphate of ATP (**Fig. S3**). Thus, for Arg177 to act as the arginine finger and catalyze hydrolysis *in trans*, the interface would require significant rearrangements.

Another positively charged residue, Lys133, is better positioned to interact *in trans* with the expected position of the γ-phosphate of ATP. Such interaction would require significantly fewer structural rearrangements. Further, Lys133 corresponds to the arginine finger identified in the bacteriophage P74-26 packaging ATPase (Hilbert et al., 2015), indicating that Lys133 may function as a "lysine finger." We note that the use of a lysine to catalyze hydrolysis *in trans* instead of the "traditional" arginine finger has been observed in both RecA (Cox et al., 2006) and DnaC (Mott et al., 2008) ATPases, and thus there is precedence for a lysine finger in ATPase ring motors.

The DNA pore

The pore of the pentameric assembly through which DNA translocates is lined with several positively charged residues (**Fig. S4**). In the C-terminal domain, Lys332 and Lys336 point directly toward the channel lumen, and are thus well positioned to interact with DNA. A slight rotation of the C-terminal domain relative to the N-terminal domain would cause these side-chains to rotate out of the channel center and position Lys333, Lys334, and Lys366 in the lumen. Hence, it is possible that both sets of residues play a role in the packaging process, though possibly in different stages of the mechano-chemical cycle. This possibility is supported by our recent cryo-EM structure of φ29 particles imaged during packaging, which showed that residues approximately equivalent to Lys333, Lys334, and Lys366 interact with the substrate DNA during the dwell phase, presumably to prevent DNA slippage while the motor resets and exchanges ADP for ATP (Mahler et al., 2020;

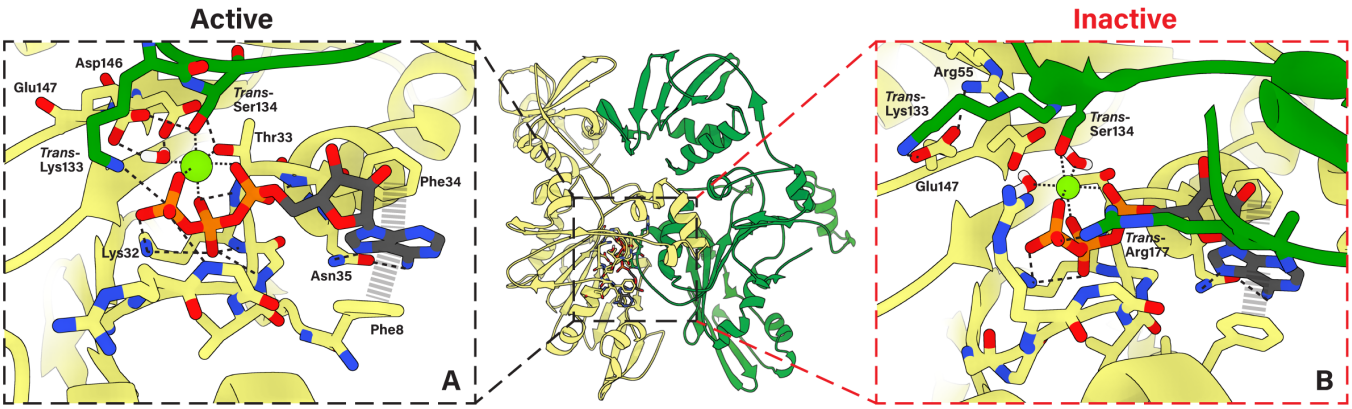

Figure 2: ATP-binding poses predicted from MD simulations. A. Active ATP-binding pocket contains canonically predicted interactions. The cis-acting (yellow) subunit's Walker A motif backbone NH groups bind the β-phosphate, Lys32 binds the γ- and β-phosphates, and Thr33 chelates Mg^{2+}. Downstream of the Walker A motif, Phe34 and Asn35 function as the Q-motif, and bind the adenosine with help from N-terminal gate Phe8. The Walker B motif Asp146 and catalytic Glu147 isolate a single water molecule, which chelates Mg^{2+} (green sphere). Residues donated in trans from the neighboring subunit (green) also participate in ATP-binding. Notably, Lys133 is seen interacting with the γ-phosphate and Ser134 chelates Mg^{2+}. **B.** Inactive pose maintains many of the same interactions as the active pose, with a few key differences. Arg177 is now donated in trans to interact with the γ-phosphate, while Lys133 interacts with catalytic Glu147 away from the γ-phosphate. This interaction is stabilized by cis-acting Arg55.

Woodson et al., 2020). Hence, these residues likely function similarly in asccφ28.

A number of additional postively charged residues from the N-terminal (ATPase) domain line the pore of the pentameric ring, namely Lys66, Lys92, Lys107, Arg110, and Arg128 (**Fig. 1**). While N-terminal domain-DNA interactions will be described in greater depth below, it is worth noting that these residues are well-conserved among other packaging ATPases, suggesting a conserved function (**Table S2**). Indeed, it was previously shown that Arg101 from the bacteriophage P74-26 packaging ATPase, analogous Arg110 in asccφ28, is absolutely necessary to bind substrate DNA (Hilbert et al., 2015, 2017), suggesting a direct role in DNA translocation. The position of this residue in the interior of the pore supports this assignment.

Motor dynamics

While the X-ray crystallographic structures described above provide valuable information regarding the tertiary and quaternary structures of a functional, DNA packaging motor, the structures were determined in the absence of nucleotide and DNA. As a result, insights into some of the most important mechanistic questions concerning the nature of force generation and the molecular basis of subunit coordination are limited. Thus, we employed long time-scale MD simulations to understand how ATP binding, hydrolysis, and product release are coordinated and coupled to DNA translocation.

ATP binding and regulation of hydrolysis

To understand how subunits around the ring bind ATP, and how this binding might modulate DNA gripping, we initially docked Mg^{2+}-ATP into each subunit based on the structure of the BeF_3-ADP-bound phage P74-26 packaging ATPase (Hilbert et al., 2015), and positioned a 30-bp, B-form dsDNA in the central pore of the pentamer. The structure was equilibrated and its equilibrium dynamics were sampled *via* MD simulations for 2.4 μs. Our simulation predicted that Mg^{2+}-ATP binds to the *cis*-acting side of the inter-subunit active site via canonical interactions with the Walker A motif: 1) the β-phosphate of ATP forms several hydrogen bonds with the backbone nitrogens of the Walker A motif; 2) the critical P-loop Lys32 coordinates the β- and γ-phosphates; and 3) Thr33 chelates the Mg^{2+} ion (**Fig. 2A**). The *cis*-acting Walker B motif residues engage in similar conserved canonical interactions: 1) Asp146 chelates the Mg^{2+} ion through a water molecule, and 2) Asp146 hydrogen bonds to the Walker A Thr33, which has

been previously predicted to be a key interaction that helps close the active site as part of the tight-binding process in viral packaging and other ATPases (delToro et al., 2019; Yang et al., 2008).

The simulation further predicted that the *trans*-acting residues donated from the neighboring subunit form a tight hydrogen bonding network with the *cis*-acting Walker motifs that is centered around the γ-phosphate (**Fig. 2A**). *Trans*-acting Lys133 hydrogen bonds to the γ-phosphate of ATP, consistent with Lys133 functioning analogously to "arginine fingers" decribed in other systems. Such an interaction would help polarize the P-O bond, and stabilize the negative charge on the departing inorganic γ-phosphate upon hydrolysis (Erzberger and Berger, 2006). Further, the residue immediately downstream of Lys133, Ser134, chelates the Mg^{2+} ion *in trans*, occupying an octahedral-coordination site typically occupied by a water molecule in previous simulations of viral packaging ATPases (delToro et al., 2019; Ortiz et al., 2019). This lysine-serine pair is distinct from SRC motifs found in many AAA+ motors that contain an arginine finger (Davey et al., 2002). In the AAA+ SRC motif, the serine residue is upstream of the *trans*-acting catalytic residue, and does not chelate Mg^{2+}. Thus, to the best of our knowledge, our structure and simulations predict a new motif for *trans*-activated catalysis in ASCE enzymes. This serine-lysine combination is also observed in the packaging ATPases from the φ29 and Sf6 bacteriophages, suggesting commonality amongst viral DNA packaging enzymes (**Fig. S5**).

Lastly, the simulations predict the *cis*-acting Walker B catalytic Glu147 hydrogen bonds to this *trans*-acting Ser134. The consequence of these interactions is a tight hydrogen bonding network centered around a single water molecule. The hydrogen atoms of this caged water H-bond with the oxygens on the 146-DE-147 carboxylate groups, whereas the oxygen atom chelates the Mg^{2+} ion. Such a configuration would polarize electron density onto the oxygen atom. Hence, the water molecule is primed for deprotonation by Glu147, with the resulting nucleophilic hydroxide ion poised for attack at the γ-phosphate as described above. It is interesting to consider the conservation of the DE pair in packaging ATPases in light of our structures and simulation; the geometry of the active site ensures that the glutamate is positioned such that deprotonation leaves the lone pair of electrons on the nucleophilic hydroxide pointing directly at the phosphate target. If the positions of Asp and Glu were switched, the hydroxide ion would not be optimally oriented for nucleophilic attack. Indeed, DE switch mutations in terminases typically abrogate ATPase activity (Mao et al., 2016b; Sun et al., 2007).

In addition to the hydrolysis-competent active site described above, our simulation suggests that the binding interface can also adopt an "inactive" conformation. This conformation is characterized by the positioning of the catalytic Glu147 away from the γ-phosphate and towards *cis*-acting Arg55. The resuting interaction between Glu147 and Arg55 is analogous to the "glutamate switch" interaction found in AAA+ motor enzymes, and is indicative of a binding interface that is in a catalytically incompetent pose (Zhang and Wigley, 2008). A similar interaction is found in crystal structures of the φ29 and Sf6 packaging ATPases with bound nucleotide (**Fig. S6**). We also found that while Ser134 still chelates Mg^{2+} *in trans* in the inactive confromation, Lys133 no longer hydrogen bonds with the ATP γ-phosphate and instead interacts with Glu147, helping Arg55 stabilize the inactive pose of the binding interface. Interestingly, Arg177, which is analogous to the previously identified arginine finger Arg146 in the φ29 packaging ATPase, now interacts with the γ-phosphate. Thus, this arginine is capable of reaching the γ-phosphate, but only when our simulation predicted a catalytically inactive binding interface. This suggests that Arg177 (and thus potentially φ29 Arg146 as well) senses nucleotide occupancy *in trans* but does not catalyze hydrolysis.

The adenosine base of ATP binds similarly in both the "inactive" and "active" interfaces (**Fig. 2A,B**). An aromatic residue immediately downstream of the canonical Walker A motif, Phe34, π-stacks with the adenosine base. The adenosine forms bidentate hydrogen bonds with the next residue, Asn35. A pairing of an aromatic residue followed by

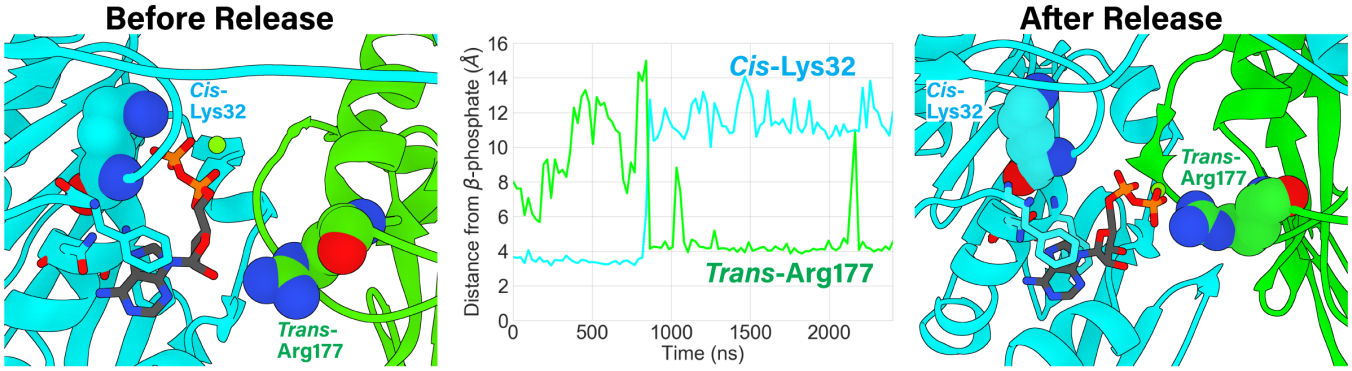

Figure 3: ADP-release is promoted by a trans-acting exchange residue. ADP unbinding is characterized by dissociation of the β-phosphate from the *cis*-acting Walker A Lys32 (interaction shown left panel) and concomitant association (time-evolved distance shwon middle panel) of the β-phosphate to *trans*-acting Arg177 (interaction shown right panel), which is implicated as being the exchange residue. Residues interacting with the adenosine (Phe8, Phe34, Asn35, shown unlabeled) largely maintain their interactions, acting as a pivot point to remove the phosphates from the binding pocket. The *cis*-acting Lys32 and *trans*-acting Arg177 are shown as spheres and are labeled. The *cis*-acting enzyme is light blue, and the *trans*-acting enzyme is green.

a carboxamide has been previously identified as the "Q motif" in viral packaging ATPases. The pair's function was implicated in binding the adenosine ring in the λ phage packaging ATPase (Tsay et al., 2009). Although in the λ phage packaging ATPase, the Q motif is located upstream of the Walker A motif, 34-FN-35 seems to perform an analogous role binding adenosine in the φ28 system. Lastly, the N-terminal loop repositions itself so that Phe8 π-stacks on the side of the adenosine opposite of Phe34. This contrasts with the position of the N-terminal loop in the crystal structure, which positions Phe8 farther away from the Walker A motif. Thus, the N-terminal loop forms a gate that can either open to allow nucleotide exchange, or close to tightly bind ATP. Similar π-stacking sandwiches flanking either side of adenosine have been observed in recently solved structures of other ATPases, such as *E. coli* MutS and the Human Catalytic Step I Spliceosome (Bhairosing-Kok et al., 2019; Zhan et al., 2018), suggesting that similar active-site gating mechanisms may be present in other ring ATPases.

Nucleotide exchange

The ATP-bound MD simulations described above show how individual subunit interfaces can bind and hydrolyze ATP. To understand what happens upon completion of the translocation burst, we simulated the structure of gp11 with ADP bound in each active site. To initiate these simulations, we started with the same initial configuration as in the ATP-bound structure described above, but removed the γ-phosphate of each ATP to generate an all ADP-bound starting structure. Presumably this structure corresponds to the state of the motor at the end of the burst/beginning of the dwell, when all five ATPs have hydrolyzed, and ADP remains bound to each active site. The system was again equilibrated and its equilibrium dynamics were simulated for at least 2.4 μs. Over this long sampling period, we captured the initial steps of ADP-release as the first subunit in the ring initiates nucleotide exchange. The event is characterized by the α- and β-phosphates of ADP detaching from the Walker A phosphate-binding motifs, while maintaining the aromatic interactions with adenosine. Release of the β-phosphate by the Walker A Lys32 is accompanied by concomitant association of the β-phosphate to the *trans*-acting Arg177 (**Fig. 3, Movie S1**). This agrees with recent assignment that the analogous φ29 Arg146 is critical for nucleotide exchange (Tafoya et al., 2018). After the phosphates are released from the Walker A motif, the flexible Walker A backbone immediately repositions backbone-NH groups such that they can no longer bind the β-phosphate of ATP/ADP (**Movie S2**). This prevents ADP from accessing energetically favorable hydrogen bonding with the Walker A motif, reducing overall nucleotide affinity and likely precipitating complete dissociation of ADP from the enzyme active site. This phenomena has been characterized in myosin motors (Porter et al., 2020), where propensity of

the Walker A motif to adopt a pose that is not receptive to β-phosphate hydrogen bonding is reported to be a predictor of ADP release rates.

Additionally, *trans*-acting loops must move substantially to provide a pathway for ADP release. This occurs when the backbone of the *cis*-acting subunit's lid subdomain rotates away from the ATPase active site. This rotation could either actively pull the *trans*-acting loops of the nieghboring subunit with it, or passively move these loops by relieving the tension imposed by the lid subdomain in the ATP-bound configuration. This agrees well with prior structual, biochemical, and simulation data that suggest both ATP binding and nucleotide release actuate rotation of the lid subdomain (Hilbert et al., 2015; Ortiz et al., 2019).

While our simulation was long compared to typical MD simulations, it was not long enough to predict diffusion of ADP into solution. Nonetheless, we were interested in understanding further structural rearrangements that might occur upon complete dissociation of ADP. Thus, we performed additional simulations to probe the conformation and dynamics of a 4-ADP-bound, 1-apo subunit-occupancy mixture by removing the partially-unbound ADP described above from the system altogether. While we did not observe significant quaternary structural rearrangements on the ~2.4 μs timescale sampled, we did observe that the apo subunit's Walker A motif backbone rearranges to position the Walker A Val30 in the "blocking" pose observed in the iodine crystal structure described above (**Movie S3**). Thus our simulation suggests that this pose may not be an artifact caused by iodine binding, but rather may be a mechanism that regulates ADP release and subsequent ATP binding.

Nucleotide-dependent DNA interaction

It is well known that the affinity for polymer substrates in ring ATPases depends on whether the ATPase active site is empty or if it has ATP or ADP bound. However, the structural basis for these changes in affinity is poorly understood. Thus, to assess the motor's nucleotide-dependent affinity for substrate DNA, we systematically compared the DNA-binding residues from the ATP- and ADP-bound simulations described above, which included DNA in the pore. Additionally, we performed an equivalent 2.4 μs simulation of an apo pentamer with substrate DNA positioned in the pore to serve as a reference. We observed that both the orientation of the positively charged residues and the overall shape of the pore depend on nucleotide occupancy of the ATPase interfacial active sites. Amongst the positively charged residues located in the lumen, we find Arg110 is the primary DNA contacting residue, consistent with this residue being the only strictly conserved positively charged residue in all solved dsDNA viral packaging ATPases (**Table S2**). Interestingly, the orientation of Arg110 is directly affected by nucleotide occupancy (**Fig. 4A**). In the all-apo simulation, all but one Arg110 lay flat along the

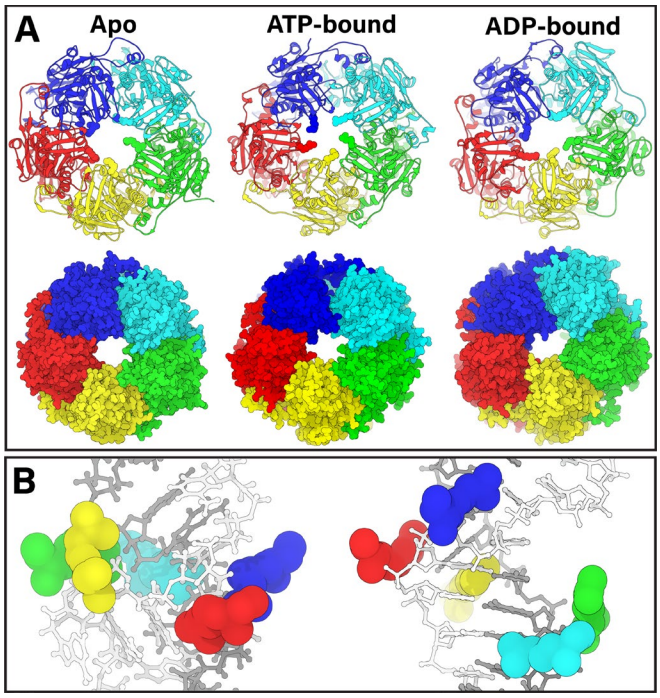

Figure 4: Pore geometry is modulated by nucleotide occupancy. A. Pentamer complex simulated in apo, ATP-bound, and ADP-bound states with substrate DNA (not shown for easier visualization) as Richardson diagrams (**top row**) and space-filling representations (**bottom row**). In the Richardson diagrams, Arg110 is shown as spheres to highlight its contribution towards DNA-gripping in the ATP-bound state. The pore is less constricted in the apo and ADP-bound states than the ATP-bound state, consistent with experimental data. **B**. Arg110 as predicted from the full-length subunit simulation are mostly a planar-ring and distort the DNA structure (**left**). Arg110 as predicted from ATPase-domain subunit simulation are donated following the helical pitch of DNA and do not distort the DNA structure (**right**).

interior of the pore, and do not interact strongly with DNA. When all five interfaces are bound with ATP, Arg110 is re-positioned into the pore as "prongs" that help grip DNA tightly. These prongs also distort the helicity of DNA – likely because they are donated as a planar ring and only somewhat follow the helicity of DNA (**Fig. 4B, left**). In the ADP-bound state, we find that Arg110 is not donated into the pore as well as it is in the ATP-bound state. It was previously shown in both the φ29 and T4 packaging motors that the ADP-bound state of the motor does not grip DNA as tightly as the ATP-bound state (Chemla et al., 2005; Ordyan et al., 2018). Thus, our simulations not only explain why the asccφ28 gp11 Arg110 analog in the P74-26 packaging ATPase was found to be necessary for DNA binding, but they also provide structural and energetic insight into the molecular basis of single-molecule observations.

Flexibility and variability of subunits

To quantitatively characterize the dynamics of the asccφ28 packaging ATPase obtained from our equilibrium MD simulation, we performed principal component analysis (PCA) coupled with root-mean-square fluctuation (RMSF) calculations on the alpha carbons of every residue in the gp11 ring in the different nucleotide and DNA bound states. RMSF provides us with a measure of how flexible a residue or motif is, while PCA allows us to understand whether flexibility is correlated as concerted motion along a specific direction or if the motion is essentially random (**Fig. 5, S7**).

Our analysis shows that the apo state is characterized by highly flexible N-terminal gate and lid subdomains. Flexibility of the lid subdomain can be attributed to the flexible hinges that connect the lid subdomain to the N- and C-terminal domains. Thus, the lid subdomain moves as a rigid body, allowing it to maintain inter-subunit contacts with, and impart force on, its neighboring subunit. PCA analysis indicates that the first principal component of this motion is projected in different directions across different subunits around the ring, which suggests that either the motion is random or it is affected by the subunit's interactions with its neighbors and the DNA (**Fig. S7**).

Upon ATP binding, the simulations predict that both the N-terminal gate and the lid subdomain lose flexibility, but that the first principal components of each subunit's lid subdomain motion are again projected along different directions (**Fig. S7**). These differences may be due to subtle differences in the way ATP is bound; subunits wherein adenosine binds the Q-motif have lid subdomain motion projected towards the ATPase binding site, whereas subunits wherein adenosine is not bound to the Q-motif do not. Although prior predictions suggested that the apo-to-ATP-bound transition is characterized by an "open-to-closed" transition (Ortiz et al., 2019), our simulations suggest this transition could also be characterized as a "flexible-to-rigid" state transition.

The ADP-bound state is characterized by a highly flexible N-terminal gate motif, but a rigid lid subdomain. The subunit wherein we observe the initial stages of ADP-release has a concerted rotation of the lid subdomain that is not observed in the other four subunit's principal components (**Fig. S7**). This again suggests that ATP binding/ADP unbinding causes rotation of the lid subdomain, consistent with prior predictions. The dynamics described above in the pentamer simulations are echoed by similar dynamics observed in short-timescale simulations of a single subunit in the apo, ATP-bound, and ADP-bound states (**Movies S4, S5, S6**).

In addition to modulating subunit dynamics, nucleotide occupancy also tunes the preferred conformation of each subunit, giving rise to changes in the overall conformation of the pentameric ring. To quantitatively characterize the variability of subunit structure around the ring, we calculated intra-subunit residue-residue pairwise distances for all five subunits, and plotted the standard deviation of the average distance (**Fig. 5**). In this analysis scheme, high standard deviation of average residue-residue distances indicates that the relative positions of residues vary across the five subunits; low standard deviation indicates

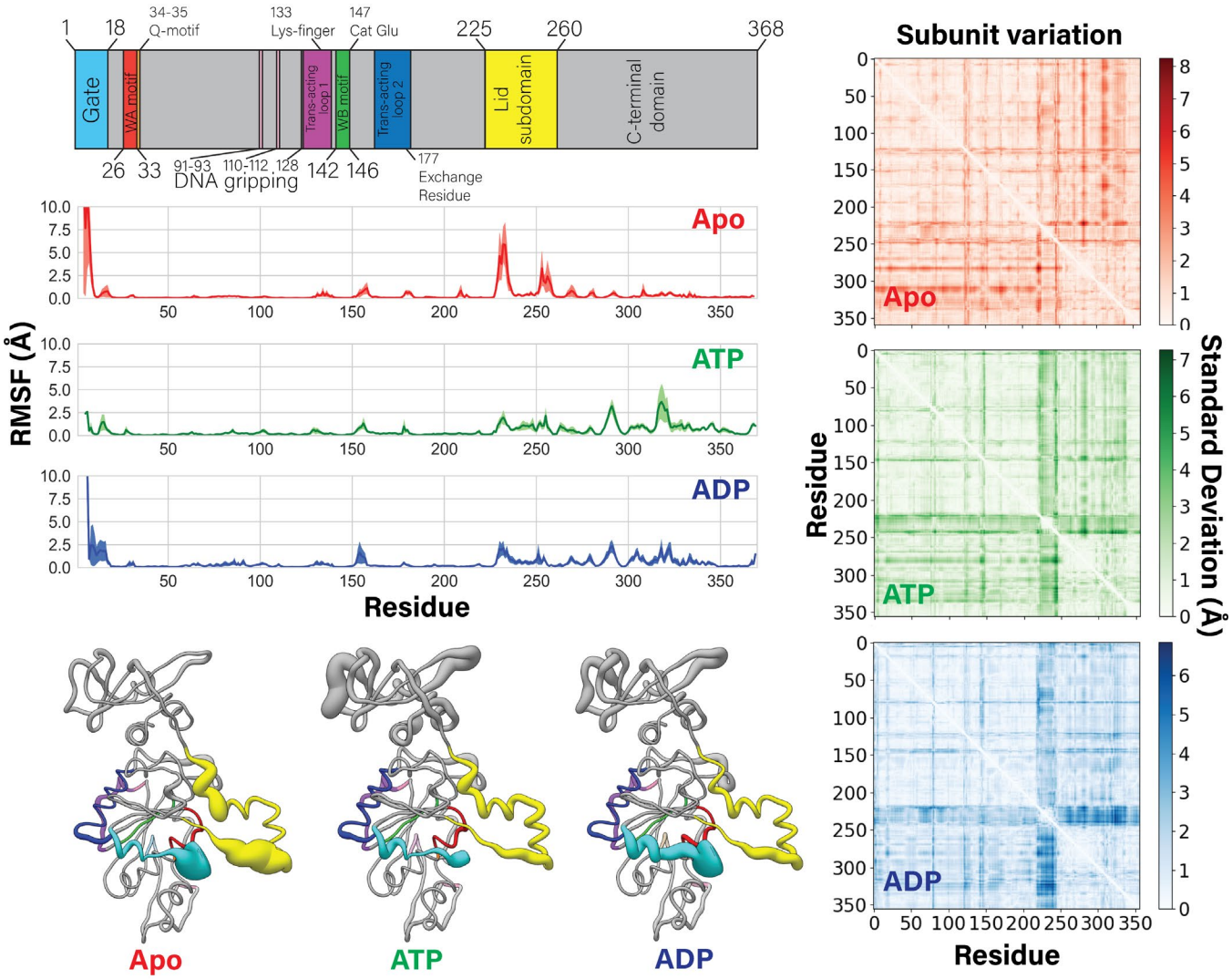

Figure 5: Flexibility of subunits is modulated by nucleotide occupancy. (**Left column**) Motif identity chart is reproduced at the top for easy reference. Averaged root-mean-square fluctuations (RMSF) of the ATPase alpha carbons over 2.4 microseconds of MD simulations are plotted. The standard error of the mean is shaded in each plot. Beneath the plots, the average RMSF value is coded to the radius of a worm-representation of the enzyme, which is color coded to the sequence. Thicker radius indicates higher flexibility. The apo state has a significantly more flexible lid subdomain than the ATP- or ADP-bound monomers. (**Right column**) Intra-subunit inter-residue distances are calculated in the apo, ATP-, and ADP-bound simulated states. The results from each of the five subunits are averaged. The standard deviations of the average are plotted as heatmaps, indicating structural variation across subunits within the pentamer. The ATP- and ADP-bound monomers have a band of high standard deviation in the lid subdomain (residues ~225-245), indicating that although each lid subdomain is rigid, they are in different poses. This band is muted in the apo state, indicating that the average positions of the lid subdomains are roughly equivalent, despite their flexibility. These observations correlate well with the asymmetry of the ATP- and ADP-bound pentamers, and the symmetry of the apo pentamer, given that the lid subdomain mediates most of the inter-subunit contacts.

structural homogeneity. The region of highest-standard deviation observed in the ATP- and ADP-bound simulated states corresponds to the lid subdomain. This result indicates that the lid subdomain of each nucleotide-bound subunit is in a unique position relative to the ATPase domain. On the other hand, this region of high standard deviation is muted in the apo simulated structure, indicating that in absence of nucleotide, each subunit's lid subdomain adopts a similar conformation. Likewise analysis of the three crystal structures shows that the gp11 ring is surprisingly asymmetric, with most of the variance again concentrated in the lid subdomain (**Fig. S8**). Since the lid subdomain mediates the majority of the inter-subunit contacts, variations in its structure

and orientation could result in different positioning of neighboring subunits and explain the asymmetric shape of the ring (**Fig. 1**).

There is a second band of significant variation, which corresponds with the *trans*-acting lysine finger and its adjacent residues (residues 130-133) (**Fig. 5**, **S8**). This observation indicates that the position of the *trans*-acting catalyic residues is modulated by the position of the neighboring subunit's lid subdomain, which directly contacts these *trans*-acting loops. Thus, nucleotide-actuated rotation of the lid subdomain is a mechanism by which the motor can rearrange its overall quaternary structure and position its neighboring subunit's *trans*-acting catalytic residues for appropriate catalytic function.

Helix tracking in viral DNA packaging ATPases

We recently solved the structure of the φ29 packaging ATPase attached to the prohead and stalled during packaging (Woodson et al., 2020). This asymmetric cryo-EM reconstruction showed that the N-terminal domains of the ATPase ring adopt a helical conformation as each subunit tracks the substrate DNA. However, the crystal structure of asccφ28 gp11 ring reported here shows no such helicity in the N- or C-terminal domains. This could be either due to crystal packing contacts forcing the ring to be planar, or lack of substrate imparting helicity on the structure. Likewise, the above MD simulations do not predict that the ATPase ring adopts a helical conformation. This is likely because the transition between the ring and helical conformations requires extension of the N- and C-terminal domains, which may have a large activation energy barrier. Thus, this transition may be kinetically infeasible to sample on the microsecond timescale.

To investigate if removal of such a barrier would allow the N-terminal domains to adopt a helical arrangement on the microsecond timescale, we simulated a pentamer ring composed of truncated monomers which contain only the N-terminal and lid (sub)domains (residues 1-260). We note that in AAA+ literature it is increasingly common to observe helical rings with truncated monomers which only contain equivalent ATPase and lid

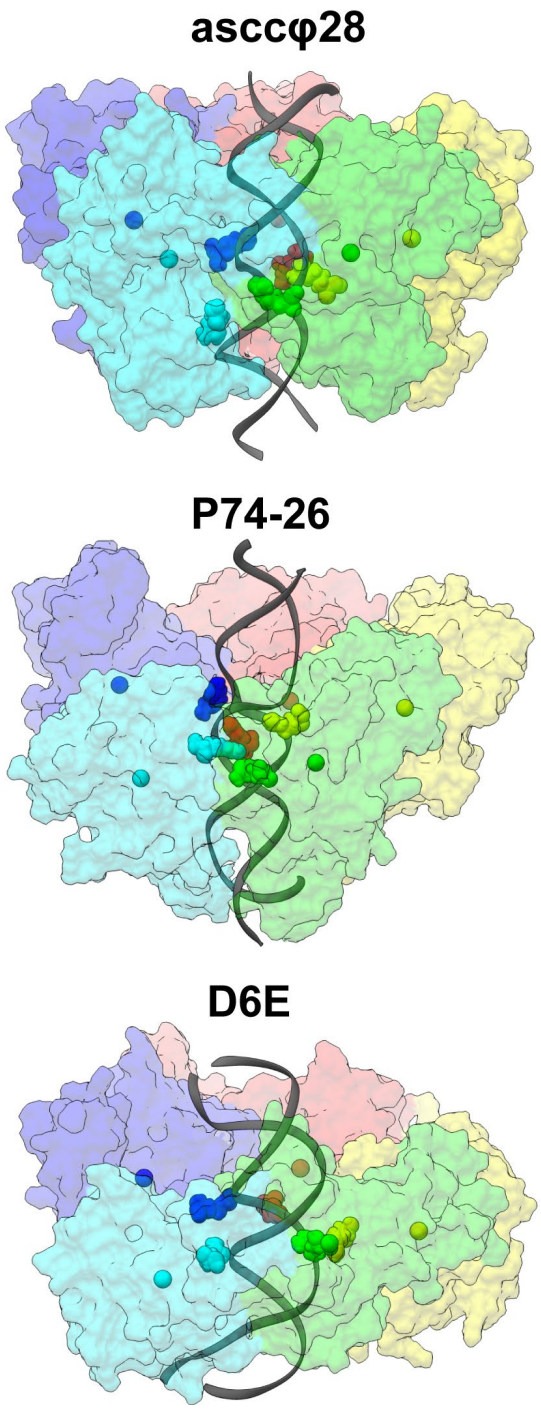

Figure 6: Helical ATPase arrangements. The predicted helical arrangements of the asccφ28, P74-26, and D6E packaging ATPases are depicted. Each subunit is shown as a transparent surface. The centers of mass of each subunit are depicted as hard spheres to show the right-handed helical arrangement descending from the blue to cyan subunits. DNA-gripping residues are shown as spheres, to show their coordination with the substrate DNA, whose phosphate backbone is a dim gray ribbon. The DNA-gripping residues of asccφ28 are the same as depicted in **Fig. 4B**.

(sub)domains (Han et al., 2020; Zehr et al., 2020). Indeed, our MD simulation of the ATP-bound asccφ28 ATPase domain assembly showed a conformational change from the planar ring assembly to a helical assembly as the subunits shifted to associate with the helical phosphate backbone of substrate DNA (**Fig. 6**). The placement of DNA-gripping residue Arg110 in the helical pose contrasts with the predicted placement from the full-length simulation (**Fig. 4B**). This helical arrangement of Arg110 better complements the helical pitch of the phosphate backbone and agrees with the placement of DNA-gripping residue Lys56 observed in our φ29 cryo-EM structure. To test if this propensity of ATPase domains to track DNA could be a general feature of viral packaging ATPases, we simulated pentamer assemblies of the P74-26 and D6E packaging ATPases constructed *in silico*. Again, our simulations predicted that these structures transition from the starting planar ring configuration to a helical configuration. (**Fig. 6**).

Whereas all three systems predicted an overall helical arrangement, the details of the arrangement vary. For example, the subunit center-of-mass helical pitch is smallest in the asccφ28 pentamer but asccφ28 DNA-gripping Arg110 tracks along the largest stretch of DNA compared to equivalent DNA-gripping residues in the P74-26 and D6E simulations. These differences in predicted helical conformations are perhaps expected, since only asccφ28 is starting from an experimentally determined structure. Thus, the P74-26 and D6E simulations have several caveats which must be considered. For instance, the lid subdomain of the P74-26 ATPase is not extended and does not facilitate as many inter-subunit contacts as the asccφ28 subunits. Additionally, placement of DNA-gripping residues may be dependent on the initial starting position of substrate DNA, which had to be manually placed into the pore. Nonetheless, our simulated structures fit well into our recently solved cryo-EM reconstruction of the φ29 motor stalled with ATP analog (**Movies S8-10**). Thus, consistent with this experimentally determined structure, we predict that viral DNA packaging motors adopt a helical arrangement as subunits track DNA.

Discussion

An emerging feature of ring ATPases is that subunits in the 'ring' arrange themselves as a helix as they track their polymeric substrates (De la Peña et al., 2018; Enemark and Joshua-Tor, 2006; Jean et al., 2020; Monroe et al., 2017; Zehr et al., 2020). From these structures, several translocation mechanisms have been proposed, and must be considered for viral DNA packaging systems as well. An essential feature of these models is that some aspect of nucleotide binding, hydrolysis, or product release triggers conformational changes that couple to directed mechanical motion, typically rotation of a smaller subdomain relative to the helix/ring.

Previously proposed mechanisms

Two compelling translocation mechanisms have been proposed based on these reported helical structures: an "inchworm" or a "hand-over-hand" mechanism. In the inchworm model, ATP hydrolysis and product release at one end of the helix cause that subunit to disengage from the polymeric substrate. ATP binding at the other end of the helix causes that subunit to engage the substrate. The net result is translocation of the polymer relative to the ring. The FtsK hexameric ATPase system is proposed to use such an inchworm mechanism, supported by a recent cryo-EM reconstruction of a hexamer stalled with ATP analog (Jean et al., 2020). In the absence of high-resolution quaternary structures, planar inchworm mechanisms had been proposed for viral DNA packaging systems as well (Hilbert et al., 2015; Sun et al., 2008; Zhao et al., 2013).

The hand-over-hand mechanism is conceptually similar to the inchworm mechanism in that movement of a subunit from one end of the helix to the other is coupled to substrate translocation. However, differences in the FtsK-like and AAA+ structures suggest different paths for this movement. In the inchworm model, the ATPase ring remains continuous as four of the six subunits adopt a helical arrangement complementary to its polymeric substrate while the remaining two subunits bridge the gap between the top and

bottom of the helix. In contrast, many AAA+ hexamers have been solved with all six subunits arranged as a helix, resulting in a discontinuous sheared interface between the bottom and top of the helix.

We considered analogous mechanisms for viral DNA packaging motors based on the observed helical arrangement in the φ29 cryo-EM reconstruction and simulated viral ATPase structures described above. However, these mechanisms are inconsistent with the well-characterized burst-dwell dynamics of the φ29 packaging ATPase (Chistol et al., 2012; Moffitt et al., 2009). Thus, we propose a distinct translocation mechanism, that accommodates these burst-dwell dynamics and our structural and simulation data.

Helical-to-planar ring translocation mechanism

We propose DNA translocation is powered by repeated "helical-to-planar" transitions of the ATPase ring motor (**Fig. 7**). This mechanism is constrained by prior SMSF studies that characterized the major features of the mechano-chemical cycle (Chemla et al., 2005; Chistol et al., 2012; Moffitt et al., 2009; Tafoya et al., 2018) and is based on: 1) the planar ring structures of asccφ28 gp11 in the absence of DNA reported here; 2) the helical structure that the closely related φ29 motor adopts when complexed with DNA and an ATP analog (Woodson et al., 2020); and 3) the MD simulations described above that inform the molecular basis of the transitions.

Mechanism of force generation: ATP binding drives two competing effects. The dominant effect is a strong interaction with the DNA phosphates, causing the ring to adopt a helical configuration as the subunits track the DNA. The second effect of ATP binding is lid subdomain rotation over the active site; because the lid subdomain is bound to a neighboring subunit, this effect drives subunits into the planar conformation. The tension between the two effects is resolved when a subunit hydrolyzes ATP to release its grip on DNA. No longer constrained by an interaction with DNA, this allows the lid subdomain of the adjacent ATP-bound neighbor to rotate and bring both subunits into a planar conformation. The result is a movement of the DNA past the hydrolyzing subunit, through the ring and into the procapsid. This forms the basis of force-generation and translocation in the packaging motor.

Burst: Our detailed description of the mechano-chemical cycle starts when all five subunits have bound ATP and therefore adopted a helical arrangement guided by the DNA substrate. In this conformation, each subunit is engaged with the DNA backbone approximately every 2 bp via Arg110 and other pore-lining positive residues (**Figs. 4 and 6**). Subunit S1 at the top of the helix hydrolyzes first and releases its grip on DNA (**Fig. 7F**), allowing subunit S2 to move up into plane with S1 (**Fig. 7G**). Since subunits S2-S5 have yet to hydrolyze ATP, they continue to grip DNA such that ~2.5 bp of DNA are translocated into the procapsid. Once S2 comes into plane with S1, S1's lysine finger (Lys133) is positioned to trigger hydrolysis in S2 (**Fig. 7G**). Hydrolysis at S2 initiates the next translocation step where another ~2.5 bp of DNA are translocated into the procapsid as subunits S3-S5 move up one position along the ATPase helix (**Fig. 7H**). The pattern repeats until S5 comes into plane with S1-S4, completing a burst and resulting in translocation of ~10 bp of DNA in 4 substeps (**Fig. 7H-J**).

Dwell: Once the motor is planar, hydrolysis at S5 would not translocate DNA (**Fig. 7J**). However, hydrolysis at this subunit is needed to release DNA and initiate nucleotide exchange (**Fig. 7A**). S5, still in plane with S1, is in position to donate its *trans*-acting exchange residue (Arg177), which promotes nucleotide exchange in S1 (**Fig 7A**). Because S1 did not move during the burst and DNA was translocated one helical turn, S1 is positioned to reengage DNA upon ATP binding. S1's exchange residue then promotes nucleotide exchange in S2 (**Fig. 7B**). Unlike S1, S2 will not be realigned with DNA in the planar conformation. However, as S2 passes through the apo state after ADP release but before ATP binding its lid subdomain is flexible, allowing the subunit to move down the helix and realign with DNA (**Fig. 7C**). We speculate that the Walker A motif may adopt the nucleotide blocking configuration described earlier (**Fig. S3, Movie S3**) to prevent nucleotide binding

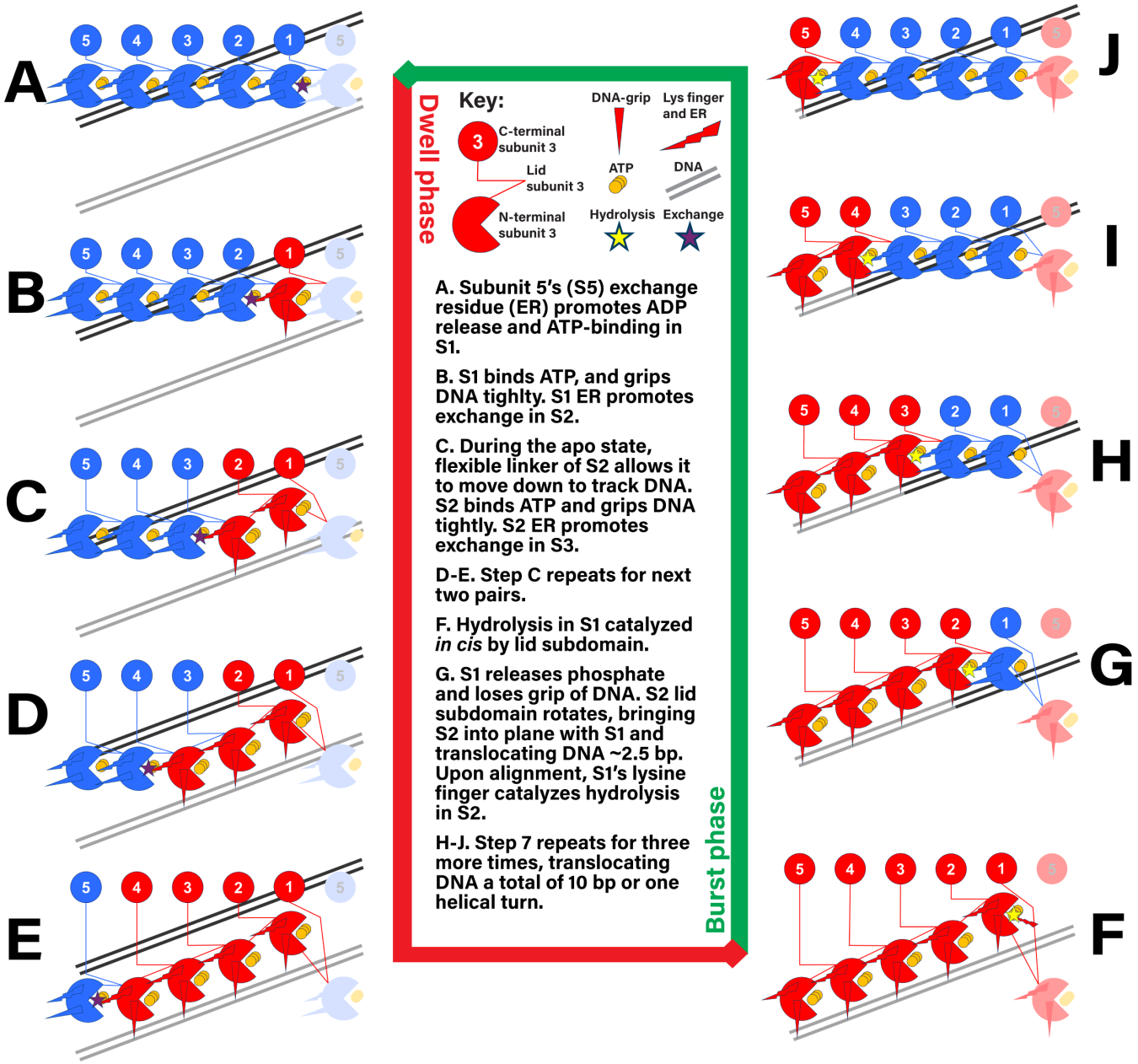

Figure 7: Helical-to-planar ring mechanism of DNA translocation. All five motor subunits numbered 1 through 5 are shown along with a periodic image of subunit 5 to indicate cyclicity, where subunits are colored red or blue to indicate ATP- or ADP-bound states. During the dwell phase (**left column, top to bottom, steps 1-5**), ADP release is sequentially and ordinally promoted by the nucleotide exchange residue. When the subunit is in a transient apo state, its lid subdomain is flexible, which allows the subunit to comes into registry with DNA. ATP binding locks the subunit in place by gripping the new helical turn of DNA and primes the lid subdomain for rotation. At the end of the dwell phase, the lid subdomain of subunit E is in a conformation which promotes self-catalysis, and this hydrolysis event begins the burst phase. During the burst phase (**right column, bottom to top, steps 6-10**), ATP hydrolysis and product release in one subunit releases grip of DNA. This enables the neighboring subunit to rotate its lid subdomain, which drives the two subunits into a planar conformation, and simultaneously drives DNA ~2.5 bp into the viral procapsid. Hydrolysis is catalyzed in trans upon alignment of two subunits.

before the subunit moves a full 2 bp down the helix. ATP binding increases S2's affinity for DNA, and thus locks it in place with respect to the DNA helix. This process occurs successively until the motor resets to the five ATP-bound, helical conformation that began the cycle (**Fig. 7C-E**).

Reinitiation of cycle: As described above, the first hydrolysis event occurs at the sheared interface, in the subunit closest to the capsid (**Fig. 7F**). The unique arrangement of this subunit's lid subdomain positions a glutamine close to the γ-phosphate, which helps to catalyze hydrolysis *in cis,* as seen in (Woodson et al., 2020). This glutamine residue is not properly positioned until the lid is positioned at the end of the dwell, and thus senses when the dwell is completed.

The helical-to-planar ring mechanism described above is consistent with the accumulated experimental data for φ29-like packaging motors. Common with the broader class of ASCE ring ATPases, our mechanism incorporates nucleotide-dependent substrate affinity (Chemla et al., 2005; Jean et al., 2020; Ordyan et al., 2018; Puchades et al., 2020). Further, our structure and simulations provide insights into the molecular basis of these observations. Specifically, the simulations show nucleotide-dependent conformational changes in DNA-gripping residues that are required to translocate DNA (**Fig. 4**). Consistent with SMFS studies (Aathavan et al., 2009; Castillo et al., 2020), our simulated asccφ28 structure and recent cryo-EM structure of φ29 particles stalled during packaging show that the ATPase subunits primarily track along a single strand of DNA (Woodson et al., 2020). Additionally, our simulations show how *cis*- and *trans*-acting residues coordinate their activities to hydrolyze (**Fig. 2**) and exchange (**Fig. 3**) nucleotide. The Lys133 and Arg177 residues assigned catalytic and exchange residue roles, respectively, agree with structural, biochemical, and biophysical characterizations of homologous residues in phage packaging systems (Hilbert et al., 2015; Tafoya et al., 2018).

While it is assumed that force is generated through conformational changes coupled to the phosphate release (Chemla et al., 2005), the nature of these conformational changes is unknown. Our model ascribes the ATP-binding induced lid subdomain rotation (**Fig. 5**), also observed in (Hilbert et al., 2015; Ortiz et al., 2019), as the force-generating conformational change. Importantly, phosphate release in one subunit releases that subunit's grip on DNA, and coordinates translocation of the neighboring DNA-bound subunit. This reconciles the otherwise paradoxical claim that ATP hydrolysis generates force within the same subunit while simultaneously causing that subunit to lose grip of DNA.

A defining feature of viral DNA packaging mechanochemistry is the biphasic burst-dwell cycle (Chistol et al., 2012; Moffitt et al., 2009), which would not emerge from the inchworm or hand-over-hand mechanisms. This key feature naturally emerges from our helical-to-planar ring translocation mechanism. Compaction of the ring from helical-to-planar is the translocation burst (**Fig. 7F-J**), while extension of the ring from planar-to-helical is the nucleotide-exchange dwell (**Fig. 7A-E**). Further, our mechanism also explains the physical basis of four translocation substeps within the context of a motor with five subunits; only four steps are required to convert the helical to the planar configuration. The last hydrolysis event (**Fig. 7J**), would not translocate DNA but coordinates nucleotide exchange, consistent with SMFS (Chistol et al., 2012). Additionally, the step size of the motor is set by the rise of the N-terminal domain helix, and thus need not be coupled to an integral number of base pairs. The small discrepancy between the 2 bp registry of subunits and the measured 2.5 bp translocation step is resolved when one also considers the internal conformational changes associated with lid subdomain rotation, as described above.

At the end of the burst, DNA is translocated one helical turn and is thus realigned with S1, the subunit that started the burst. This subunit reengages DNA to hold it in place while the remaining subunits drop down the helix mediated by interlaced nucleotide exchange. This highlights the importance of critical electrostatic contacts every 10 bp, or one helical turn, of DNA observed in (Aathavan et al., 2009). Recent SMFS studies of

the φ29 system packaging RNA and DNA/RNA hybrids showing that the burst size readjusts to the periodicity of the substrate (Castillo et al., 2020), supporting a helical-to-planar translocation mechanism.

Our proposed model represents the first atomistic description of a viral DNA packaging mechanism. This model is supported by an atomic-resolution structure of the ATPase pentamer assembly along with an asymmetric cryo-EM reconstruction of the entire motor complex and long timescale MD simulations. Unlike other mechanisms, our helical-to-planar ring mechanism naturally gives rise to burst-dwell dynamics. We note that similar burst-dwell dynamics have been observed in the ClpX protein degradation machinery (Sen et al., 2013). Additionally, planar and helical conformations have been observed for other ATPases, suggesting that our mechanism could broadly apply.

Acknowledgments

This work was supported by Public Health Service grant GM122979 (to P.J.J. and M.C.M.), GM127365 (to M.C.M.), National institutes of Health (NIH) R01GM118817 (to G.A.), and National Science Foundation MCB1817338 (to B.A.K.). Computational resources for short equilibration simulations were provided by the NSF XSEDE Program ACI-1053575. Anton 2 computer time was provided by the Pittsburgh Supercomputing Center (PSC) through Grant R01GM116961 from the National Institutes of Health. The Anton 2 machine at PSC was generously made available by D.E. Shaw Research. The authors declare no conflict of interest.

Aathavan, K., Politzer, A.T., Kaplan, A., Moffitt, J.R., Chemla, Y.R., Grimes, S., Jardine, P.J., Anderson, D.L., and Bustamante, C. (2009). Substrate interactions and promiscuity in a viral DNA packaging motor. Nature *461*, 669–673.

Bhairosing-Kok, D., Groothuizen, F.S., Fish, A., Dharadhar, S., Winterwerp, H.H.K., and Sixma, T.K. (2019). Sharp kinking of a coiled-coil in MutS allows DNA binding and release. Nucleic Acids Research gkz649.

Casjens, S.R. (2011). The DNA-packaging nanomotor of tailed bacteriophages. Nature Reviews. Microbiology *9*, 647–657.

Castillo, J.P., Tong, A., Tafoya, S., Jardine, P.J., and Bustamante, C. (2020). A DNA translocase operates by cycling between planar and lock-washer structures (bioRxiv).

Chemla, Y.R., Aathavan, K., Michaelis, J., Grimes, S., Jardine, P.J., Anderson, D.L., and Bustamante, C. (2005). Mechanism of force generation of a viral DNA packaging motor. Cell *122*, 683–692.

Chistol, G., Liu, S., Hetherington, C.L., Moffitt, J.R., Grimes, S., Jardine, P.J., and Bustamante, C. (2012). High Degree of Coordination and Division of Labor among Subunits in a Homomeric Ring ATPase. Cell *151*, 1017–1028.

Cox, J.M., Abbott, S.N., Chitteni-Pattu, S., Inman, R.B., and Cox, M.M. (2006). Complementation of One RecA Protein Point Mutation by Another: EVIDENCE FOR TRANS CATALYSIS OF ATP HYDROLYSIS. J. Biol. Chem. *281*, 12968–12975.

Davey, M.J., Jeruzalmi, D., Kuriyan, J., and O'Donnell, M. (2002). Motors and switches: AAA+ machines within the replisome. Nat Rev Mol Cell Biol *3*, 826–835.

De la Peña, A.H., Goodall, E.A., Gates, S.N., Lander, G.C., and Martin, A. (2018). Substrate-engaged 26S proteasome structures reveal mechanisms for ATP-hydrolysis–driven translocation. Science *362*.

delToro, D., Ortiz, D., Ordyan, M., Pajak, J., Sippy, J., Catala, A., Oh, C.-S., Vu, A., Arya, G., Smith, D.E., et al. (2019). Functional Dissection of a Viral DNA Packaging Machine's Walker B Motif. Journal of Molecular Biology *431*, 4455–4474.

Ding, F., Lu, C., Zhao, W., Rajashankar, K.R., Anderson, D.L., Jardine, P.J., Grimes, S., and Ke, A. (2011). Structure and assembly of the essential RNA ring component of a viral DNA packaging motor. Proceedings of the National Academy of Sciences *108*, 7357–7362.

Enemark, E.J., and Joshua-Tor, L. (2006). Mechanism of DNA translocation in a replicative hexameric helicase. Nature *442*, 270–275.

Erzberger, J.P., and Berger, J.M. (2006). Evolutionary relationships and structural mechanisms of AAA+ proteins. Annu. Rev. Biophys. Biomol. Struct. *35*, 93–114.

Finer, J.T., Simmons, R.M., and Spudich, J.A. (1994). Single myosin molecule mechanics: piconewton forces and nanometre steps. Nature *368*, 113–119.

Fuller, D.N., Raymer, D.M., Rickgauer, J.P., Robertson, R.M., Catalano, C.E., Anderson, D.L., Grimes, S., and Smith, D.E. (2007a). Measurements of Single DNA Molecule Packaging Dynamics in Bacteriophage λ Reveal High Forces, High Motor Processivity, and Capsid Transformations. Journal of Molecular Biology *373*, 1113–1122.

Fuller, D.N., Raymer, D.M., Kottadiel, V.I., Rao, V.B., and Smith, D.E. (2007b). Single phage T4 DNA packaging motors exhibit large force generation, high velocity, and dynamic variability. Proceedings of the National Academy of Sciences *104*, 16868–16873.

Glynn, S.E., Martin, A., Nager, A.R., Baker, T.A., and Sauer, R.T. (2009). Structures of Asymmetric ClpX Hexamers Reveal Nucleotide-Dependent Motions in a AAA+ Protein-Unfolding Machine. Cell *139*, 744–756.

Grimes, S., Jardine, P.J., and Anderson, D. (2002). Bacteriophage φ29 DNA packaging.

Han, H., Fulcher, J.M., Dandey, V.P., Iwasa, J.H., Sundquist, W.I., Kay, M.S., Shen, P.S., and Hill, C.P. (2019). Structure of Vps4 with circular peptides and implications for translocation of two polypeptide chains by AAA+ ATPases. ELife *8*, e44071.

Han, H., Schubert, H.L., McCullough, J., Monroe, N., Purdy, M.D., Yeager, M., Sundquist, W.I., and Hill, C.P. (2020). Structure of spastin bound to a glutamate-rich peptide implies a hand-over-hand mechanism of substrate translocation. J. Biol. Chem. *295*, 435–443.

Hilbert, B.J., Hayes, J.A., Stone, N.P., Duffy, C.M., Sankaran, B., and Kelch, B.A. (2015). Structure and mechanism of the ATPase that powers viral genome packaging. Proceedings of the National Academy of Sciences *112*, E3792–E3799.

Hilbert, B.J., Hayes, J.A., Stone, N.P., Xu, R.G., and Kelch, B.A. (2017). The large terminase DNA packaging motor grips DNA with its ATPase domain for cleavage by the flexible nuclease domain. Nucleic Acids Research *45*, 3591–3605.

Jean, N.L., Rutherford, T.J., and Löwe, J. (2020). FtsK in motion reveals its mechanism for double-stranded DNA translocation. Proc Natl Acad Sci USA *117*, 14202–14208.

Koti, J.S., Morais, M.C., Rajagopal, R., Owen, B.A., McMurray, C.T., and Anderson, D.L. (2008). DNA packaging motor assembly intermediate of bacteriophage φ29. Journal of Molecular Biology *381*, 1114–1132.

Kotsonis, S.E., Powell, I.B., Pillidge, C.J., Limsowtin, G.K., Hillier, A.J., and Davidson, B.E. (2008). Characterization and genomic analysis of phage asccφ28, a phage of the family Podoviridae infecting Lactococcus lactis. Applied and Environmental Microbiology *74*, 3453–3460.

Mahler, B.P., Bujalowski, P.J., Mao, H., Dill, E.A., Jardine, P.J., Choi, K.H., and Morais, M.C. (2020). NMR structure of a vestigial nuclease provides insight into the evolution of functional transitions in viral dsDNA packaging motors (Biophysics).

Mao, H., Reyes-Aldrete, E., Sherman, M.B., Woodson, M., Atz, R., Grimes, S., Jardine, P.J., and Morais, M.C. (2016a). Structural and Molecular Basis for Coordination in a Viral DNA Packaging Motor. Cell Rep *14*, 2017–2029.

Mao, H., Saha, M., Reyes-Aldrete, E., Sherman, M.B., Woodson, M., Atz, R., Grimes, S., Jardine, P.J., and Morais, M.C. (2016b). Structural and Molecular Basis for Coordination in a Viral DNA Packaging Motor. Cell Reports *14*, 2017–2029.

Moffitt, J.R., Chemla, Y.R., Aathavan, K., Grimes, S., Jardine, P.J., Anderson, D.L., and Bustamante, C. (2009). Intersubunit coordination in a homomeric ring ATPase. Nature *457*, 446–450.

Monroe, N., Han, H., Shen, P.S., Sundquist, W.I., and Hill, C.P. (2017). Structural basis of protein translocation by the Vps4-Vta1 AAA ATPase. ELife *6*, 1–22.

Morais, M.C. (2012). The dsDNA packaging motor in bacteriophage ø29. In Viral Molecular Machines, (Springer), pp. 511–547.

Morais, M.C., Choi, K.H., Koti, J.S., Chipman, P.R., Anderson, D.L., and Rossmann, M.G. (2005). Conservation of the capsid structure in tailed dsDNA bacteriophages: the pseudoatomic structure of φ29. Molecular Cell *18*, 149–159.

Morais, M.C., Koti, J.S., Bowman, V.D., Reyes-Aldrete, E., Anderson, D.L., and Rossmann, M.G. (2008). Defining Molecular and Domain Boundaries in the Bacteriophage φ{symbol}29 DNA Packaging Motor. Structure *16*, 1267–1274.

Mott, M.L., Erzberger, J.P., Coons, M.M., and Berger, J.M. (2008). Structural Synergy and Molecular Crosstalk between Bacterial Helicase Loaders and Replication Initiators. Cell *135*, 623–634.

Ogura, T., Whiteheart, S.W., and Wilkinson, A.J. (2004). Conserved arginine residues implicated in ATP hydrolysis, nucleotide-sensing, and inter-subunit interactions in AAA and AAA+ ATPases. Journal of Structural Biology *146*, 106–112.

Ordyan, M., Alam, I., Mahalingam, M., Rao, V.B., and Smith, D.E. (2018). Nucleotide-dependent DNA gripping and an end-clamp mechanism regulate the bacteriophage T4 viral packaging motor. Nature Communications *9*.

Ortiz, D., delToro, D., Ordyan, M., Pajak, J., Sippy, J., Catala, A., Oh, C.-S., Vu, A., Arya, G., Feiss, M., et al. (2019). Evidence that a catalytic glutamate and an 'Arginine Toggle' act in concert to mediate ATP hydrolysis and mechanochemical coupling in a viral DNA packaging motor. Nucleic Acids Research *47*, 1404–1415.

Pajak, J., Arya, G., and Smith, D.E. (2019). Biophysics of DNA Packaging. In Reference Module in Life Sciences, (Elsevier), p. B9780128096338209000.

Porter, J.R., Meller, A., Zimmerman, M.I., Greenberg, M.J., and Bowman, G.R. (2020). Conformational distributions of isolated myosin motor domains encode their mechanochemical properties. ELife *9*, e55132.

Puchades, C., Sandate, C.R., and Lander, G.C. (2020). The molecular principles governing the activity and functional diversity of AAA+ proteins. Nat Rev Mol Cell Biol *21*, 43–58.

Rao, V.B., and Feiss, M. (2015). Mechanisms of DNA Packaging by Large Double-Stranded DNA Viruses. Annual Review of Virology *2*, 351–378.

Sen, M., Maillard, R.A., Nyquist, K., Rodriguez-Aliaga, P., Pressé, S., Martin, A., and Bustamante, C. (2013). The ClpXP Protease Unfolds Substrates Using a Constant Rate of Pulling but Different Gears. Cell *155*, 636–646.

Simpson, A.A., Tao, Y., Leiman, P.G., Badasso, M.O., He, Y., Jardine, P.J., Olson, N.H., Morais, M.C., Grimes, S., Anderson, D.L., et al. (2000). Structure of the bacteriophage φ29 DNA packaging motor. Nature *408*, 745–750.

Smith, D.E., Tans, S.J., Smith, S.B., Grimes, S., Anderson, D.L., and Bustamante, C. (2001). The bacteriophage phi 29 portal motor can package DNA against a large internal force. Nature *413*, 748–752.

Sun, S., Kondabagil, K., Gentz, P.M., Rossmann, M.G., and Rao, V.B. (2007). The Structure of the ATPase that Powers DNA Packaging into Bacteriophage T4 Procapsids. Molecular Cell *25*, 943–949.

Sun, S., Kondabagil, K., Draper, B., Alam, T.I., Bowman, V.D., Zhang, Z., Hegde, S., Fokine, A., Rossmann, M.G., and Rao, V.B. (2008). The Structure of the Phage T4 DNA Packaging Motor Suggests a Mechanism Dependent on Electrostatic Forces. Cell *135*, 1251–1262.

Svoboda, K., Schmidt, C.F., Schnapp, B.J., and Block, S.M. (1993). Direct observation of kinesin stepping by optical trapping interferometry. Nature *365*, 721–727.

Tafoya, S., Morais, M.C., Castillo, J.P., Bustamante, C., Liu, S., Grimes, S., Jardine, P.J., and Atz, R. (2018). Molecular switch-like regulation enables global subunit coordination in a viral ring ATPase. Proceedings of the National Academy of Sciences *115*, 7961–7966.

Tsay, J.M., Sippy, J., Feiss, M., and Smith, D.E. (2009). The Q motif of a viral packaging motor governs its force generation and communicates ATP recognition to DNA interaction. Proceedings of the National Academy of Sciences *106*, 14355–14360.

Woodson, M., Pajak, J., Zhao, W., Zhang, W., Arya, G., White, M.A., Jardine, Paul.J., and Morais, M.C. (2020). A viral genome packaging motor transitions between cyclic and helical symmetry to translocate dsDNA (Biophysics).

Xu, R.-G., Jenkins, H.T., Antson, A.A., and Greive, S.J. (2017). Structure of the large terminase from

a hyperthermophilic virus reveals a unique mechanism for oligomerization and ATP hydrolysis. Nucleic Acids Research *45*, 13029–13042.

Yang, R., Scavetta, R., and bao Chang, X. (2008). The hydroxyl group of S685 in Walker A motif and the carboxyl group of D792 in Walker B motif of NBD1 play a crucial role for multidrug resistance protein folding and function. Biochimica et Biophysica Acta - Biomembranes *1778*, 454–465.

Zehr, E., Szyk, A., Piszczek, G., Szczesna, E., Zuo, X., and Roll-Mecak, A. (2017). Katanin spiral and ring structures shed light on power stroke for microtubule severing. Nat Struct Mol Biol *24*, 717–725.

Zehr, E.A., Szyk, A., Szczesna, E., and Roll-Mecak, A. (2020). Katanin Grips the β-Tubulin Tail through an Electropositive Double Spiral to Sever Microtubules. Developmental Cell *52*, 118-131.e6.

Zhan, X., Yan, C., Zhang, X., Lei, J., and Shi, Y. (2018). Structure of a human catalytic step I spliceosome. Science *359*, 537–545.

Zhang, X., and Wigley, D.B. (2008). The “glutamate switch” provides a link between ATPase activity and ligand binding in AAA+ proteins. Nature Structural and Molecular Biology *15*, 1223–1227.

Zhao, H., Christensen, T.E., Kamau, Y.N., and Tang, L. (2013). Structures of the phage Sf6 large terminase provide new insights into DNA translocation and cleavage. Proceedings of the National Academy of Sciences of the United States of America *110*, 8075–80.